Proceedings of the ASME 2023
International Mechanical Engineering Congress and Exposition
IMECE2023
October 29-November 2, 2023, New Orleans, Louisiana

IMECE2023-112373

IMPROVING EFFICIENCY OF AUTOMOTIVE COATING AND CURING PROCESSES THROUGH DEEP LEARNING ALGORITHMS AND HIGH-FIDELITY CFD MODELING

Sílvio Cândido*, Mohammad-Reza Pendar, José C. Páscoa

C-MAST, Center for Mechanical and Aerospace Science and Technology
Faculty of Engineering, University of Beira Interior
6200 Covilhã, Portugal

ABSTRACT

The automobile industry has relied on computational fluid dynamics (CFD) simulations to analyze and optimize the coating and curing processes, speed up product development, and lower the cost of product development. However, CFD modelings of these processes are computationally expensive due to the complexity of the models and the large number of simulations needed, especially when its used complex sprays such as the nithrothermal electrospray. As a result, more efficient methods must be developed to reduce computing time without compromising accuracy. In this article, we analyze how deep learning techniques can be used to predict coating and curing processes using electrospray CFD simulation. A dataset of 3D Eulerian-Lagrangian CFD simulations of coating and curing processes employing electrospray for the automotive industry has been used to train different deep-learning models. We investigated how hyperparameters such as batch size and layer count affected deep learning model performance compared to conventional CFD simulations. For this, we evaluated the deep learning models' efficiency and accuracy in terms of computing time. We also investigated how hyperparameters such as batch size and layer count affected deep learning model performance. Also, we've looked at the target's final droplet deposition, and distribution that is required to accurately estimate the distribution. Furthermore, we studied the percentage of snapshots of the droplet distribution electrospray necessary to predict the target's final deposition from the Lagrangian distribution. According to our findings, deep learning models can drastically reduce the amount of time needed to run CFD simulations. Depending on the model and hyperparameters applied, we can forecast the whole CFD simulation by utilizing somewhere between 10% and 15% of the initial spray development. Also, we discovered that the use of recurrent cells as an LSTM model outperformed the other models in terms of accuracy and computational efficiency, where the LSTM layers can extract better the features of the input snapshots. Overall, our research demonstrates the potential of deep learning techniques to significantly shorten the computing time of CFD simulations of coating and curing processes for the automotive sector. The results of this study have significant implications for coating and curing process design and optimization in the automobile industry as well as in other industries where CFD simulations are frequently employed.

*Corresponding author: silvio.candido@ubi.pt

1. INTRODUCTION

The paint shop plant in the automotive industry consumes the most energy share of overall production, and requires specific attention to enhance energy efficiency while reducing its environmental impact. In addition, the paint film must exhibit high physical quality, including corrosion resistance, aesthetic appeal, surface durability, and mechanical protection [1]. To meet these requirements, different techniques have been extensively studied to improve the coating and curing process time [2]. One recent idea is the use of nitrotherm electrostatic spray painting for the coating process. This method has an efficient superior transfer efficiency (TE) up to 90%, which can ideally reduce the process time. Additionally, it eliminates unfavorable phenomena such as overspray, unsatisfactory film quality, extreme material usage, and significant pollution levels during the coating process. Nitrotherm electrostatic spray painting has become a fundamental painting technology, particularly in the automotive and aerospace industries [2].

Given its impact on the automotive industry, numerical modeling techniques are essential tools for optimizing base concepts to meet the requirements and for gaining a deep understanding of turbulence airflow and droplet traveling mechanisms.

The use of heated nitrogen in an electrostatic spraying process is a technology already in use in rare high-tech companies, with very positive results [3]. They reported improvement in the transfer efficiency (TE) process and faster paint curing time [4], using heated nitrogen and compared it with conventional spraying

using air. This approach can reduce the paint shop's energy and material consumption. The current study considers a broad range of dominant parameters of described technologies as the process that is still ambiguous.

A powerful method for improving comprehension and predicting fluid flow behavior is the use of machine learning models in conjunction with computational fluid dynamics (CFD) simulations. To predict fluid flow behavior from a small set of input variables, such as boundary conditions or initial circumstances, one frequent method is to employ machine learning models. This can help in lowering the computational cost of running complete CFD simulations.

Recent advances in machine learning have brought a revolution in computational fluid dynamics (CFD). One typical strategy is to utilize machine learning models to forecast fluid flow behavior based on a small set of input variables, such as boundary conditions or initial circumstances [5]. Two deep learning machine learning models, Convolutional Neural Networks (CNNs) and Recurrent Neural Networks (RNNs), have demonstrated promising results in CFD applications [6]The application of modal decomposition has proven effective in extracting the main dynamics of the flow. However, it demands a thorough comprehension of the mathematical manipulations involved [7]. In contrast, deep learning models operate more like a "black box", requiring less explicit understanding of their internal processes.

Among the various machine learning approaches, Support Vector Machines (SVM), Artificial Neural Networks (ANNs), Recurrent Neural Networks (RNNs), and Convolutional Neural Networks (CNNs) have all been extensively investigated and used in a variety of study fields [8–10]. SVM is a classification technique that looks for the best line to draw between various classes. The ANN method called a feedforward network can approximate any function if it has enough hidden layers and neurons. The RNN approach can model sequence data by transferring knowledge from the prior time steps to the present one. The CNN method, a sophisticated neural network, can accurately detect spatial correlations in image data.

ANNs have been used to analyze nanofluid jet impingement heat transfer and pressure drop in microchannel heat sinks [11]. Additionally, a radial basis neural network (RBFNN) was developed and employed to model the pressure drop for a cyclone separator [12]. These models can automatically extract spatial information from the input data and learn complex fluid dynamics patterns by utilizing the convolutional layers of CNNs.

However, for CFD applications, deep learning models often require large amounts of data and computational power. Researchers have suggested several methods to overcome this problem, such as using pooling layers to downsample the input's spatial dimensions and reduce the number of model parameters [13]. Data augmentation and transfer learning can also be employed to enhance the performance of models with limited data [14].

Recurrent layers are a type of cell in these models that are useful for modeling temporal relationships in data related to fluid flow [15]. These models can record the fluid flow's temporal evolution using recurrent layers and generate predictions based on the flow's past behavior [16, 17].

The goal of this work is to introduce two novel techniques: (1) numerical simulation of the Nithrothermal spraying technique, and (2) proposal of a deep learning model based on the ANNs to reduce the computational cost of the simulations.

1.1 Problem Definition

In Figure 1, a schematic of the computational domain and boundary conditions nitro-therm electrostatic spraying for the simplified process is shown. The dominant forces that interact with droplets to achieve a TE higher than approximately 90% are described. The resulting fine and consistent disintegrated droplets achieve a high-quality finish on the target surface.

The computational domain of the electrospray is modeled as a cylinder with a diameter of 540D and a height of 70D, where D = 2.5 mm is the diameter of the liquid injection nozzle used for normalization.

2. METHODS

In this section, we discuss the numerical procedure for modeling the nitro-therm electrostatic thought CFD, which constructed our high-fidelity database to train a deep learning model.

2.1 NUMERICAL MODELLING METHODS

The CFD calculation of the electrospray is performed using a three-dimensional (3D) comprehensive Eulerian-Lagrangian algorithm, which is extended under the framework of the OpenFOAM package. This model type was selected because previous applications of a fully Eulerian algorithm for this type of electrospray proved to be extremely computationally intensive [18]. And this provides an in-depth analysis of the fully turbulent airflow field with the presence of heated nitrogen-enriched distribution. An unsteady compressible Navier-Stokes solver is combined with a Large Eddy Simulation (LES) model to accurately simulate the turbulence effects of the air or nitrogen flow field on the droplets. This is then two-way coupled with the effects of (I) electric field generation and droplet charging process, (II) dynamics and trajectory tracking of manipulated droplets, (III) primary and secondary breakup processes, (IV) atomized liquid evaporation, and (V) deposited film structure and thickness. This implementation is described with details in our previous publications [19–21].

Based on the grid independence study of the authors, the medium grid with 1.2 million overall cells showed good agreement in terms of convergence. The prism layer height is considered 1.4×10^{-4} m (at solid boundaries), for the grid to accurately capture the high-Reynolds turbulent flow mechanisms (see [22]). The turbulent flow dynamics in the boundary layer were properly captured. Additionally, a mesh sensitivity evaluation by considering the Kolmogorov power law-decay ($f^{-5/3}$) and proper capturing of turbulent flow details was obtained. Figure 2 shows the generated mesh with a total of 1.2 million cells.

Furthermore, the Courant number is kept below 0.45 and the time step is set to 0.1 μs, ensuring a suitable time step for high-precision results and faster convergence. The atmospheric boundary condition is set to define the computing domains outside of the borders.

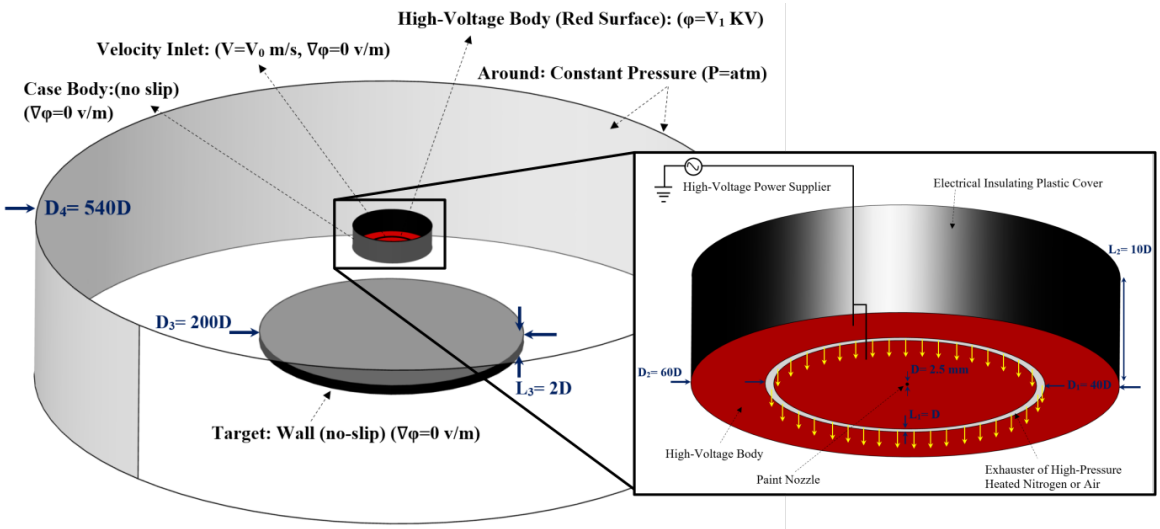

FIGURE 1: SCHEMATICS OF THE COMPUTATIONAL DOMAIN OF DESIGNED GEOMETRY FOR NITRO-THERM SPRAY TECHNIQUE ANALYSIS, WHICH A CLOSE-WINDOW ON THE INLET BODY.

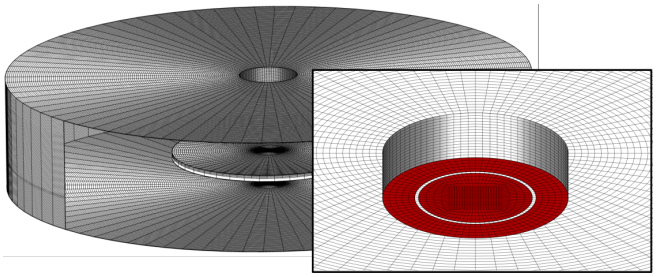

FIGURE 2: STRUCTURED GRID VISUALIZATION AROUND THE DESIGNATED GEOMETRY FOR THE NITRO-THERM SPRAYING ANALYSIS WITH A CLOSE-UP VIEW OF THE INJECTION SECTION.

2.2 MACHINE LEARNING METHODS

In our investigation, we tested different machine learning model architectures, and for each one, we studied different hyperparameters and compared the results of the optimized model. The tested models are based on the typical architecture of an Artificial Neural Network Encoder-Decoder (AE). Figure 3 illustrates the core of the methodology which is used.

Here we describe the steps for training our machine-learning model like. Creating a machine learning model to predict the flow field of an electrospray using 2D RGB images of the temporal evolution of droplets as an input would involve the following steps:

1. Collect a dataset of 2D RGB images of the temporal evolution of the droplet spray for different working conditions. These 2D images are cross-sections of the CFD results. This dataset should include a range of different working conditions, such as electric voltages, inlet velocity, temperature of the nitrogen, and charge/droplet relation.

2. Pre-process the images by resizing them to a consistent size and possibly converting them to grayscale (for better learning). It's also useful to perform image normalization to ensure that the values on all the datasets are comparable (maximum/minimum normalization).

3. Split the dataset into training, validation, and testing sets, with a proportion of around 80/20.

4. Train the model on the training and validation sets, adjusting the hyperparameters as needed to improve performance, using a chosen model architecture.

5. Evaluate the model's performance on the testing set to determine how well it can predict the flow field of the electrospray for unseen working conditions.

6. Fine-tune and optimize the model as necessary to achieve the desired level of accuracy.

The basic unit of an ANN is a neuron that takes inputs, performs computations on them, and produces outputs. The computation performed by a neuron is typically a weighted sum of its inputs followed by an activation function. Each neuron in an ANN receives inputs from other neurons or external sources and produces an output based on a weighted sum of inputs modified by a nonlinear activation function. Activation functions introduce nonlinearity into the model, allowing it to learn complex patterns and relationships in the data. The output of each neuron is passed as input to the next layer of neurons until the final output is produced. This process is called forward propagation, and it's how the model makes predictions based on the input data [16].

Neuron weights and biases are learned through a process called Backpropagation. Backpropagation adjusts the weights and biases based on the difference between the predicted output and the actual output. This process is repeated over and over on the training dataset until the model's predictions are sufficiently accurate on new data. Backpropagation algorithms minimize the loss function using common optimization algorithms such as stochastic gradient descent or ADAM optimizer.

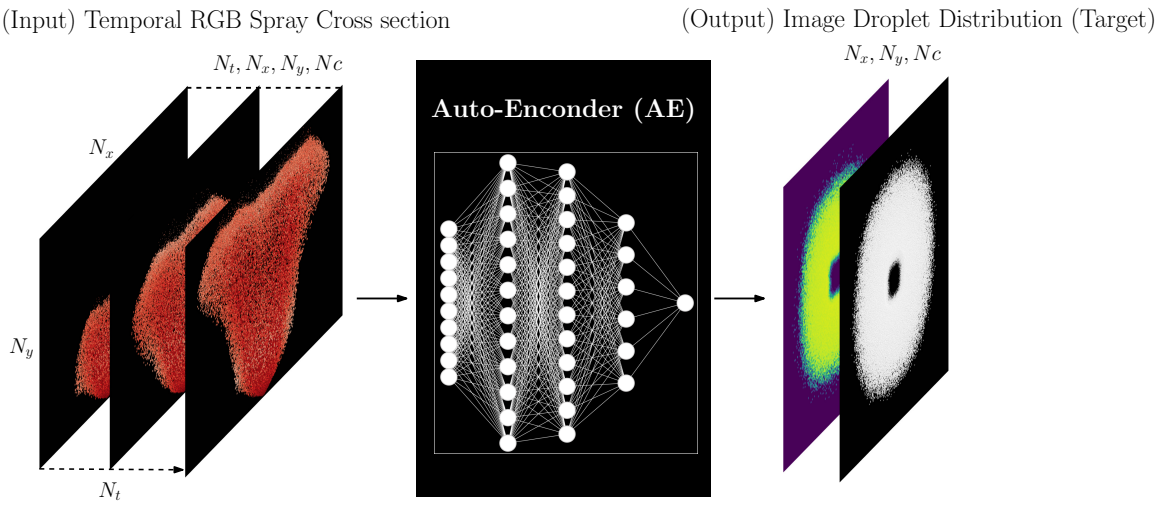

FIGURE 3: MACHINE LEARNING METHODOLOGY BASED ON ARTIFICIAL NEURAL NETWORK.

A basic ANN architecture consists of neurons connected in simple combinations. However, for temporal data, other types of layers can be used that allow for sequential input data. A recurrent neural network (RNN) model is an example of such a model. In our work, we used standard RNN models and RNNs with a specific type of repetitive cell known as LSTM (Long Short-Term Memory). Hidden layers in the RNN models are defined by mathematical formulas.

$$h_t = \sigma(W_{ih}x_t + b_{ih} + W_{hh}h_{t-1} + b_{hh}) \tag{1}$$

where, x_t is the input at time step t. h_t is the output (hidden state) at time step t. W_{ih} is the weight matrix for the input. W_{hh} is the weight matrix for the hidden state. b_{ih} and b_{hh} are the bias terms. σ is the activation function (e.g. TanH or ReLu)

The equation for a single LSTM cell (or layer) can be written as follows:

$$f_t = \sigma_g(W_f x_t + U_f h_{t-1} + b_f) \tag{2}$$
$$i_t = \sigma_g(W_i x_t + U_i h_{t-1} + b_i) \tag{3}$$
$$o_t = \sigma_g(W_o x_t + U_o h_{t-1} + b_o) \tag{4}$$
$$c_t = f_t * c_{t-1} + i_t * \sigma_c(W_c x_t + U_c h_{t-1} + b_c) \tag{5}$$
$$h_t = o_t * \sigma_h(c_t) \tag{6}$$

where x_t is the input at time t. h_{t-1} is the output of the previous LSTM layer at time $t-1$. f_t, i_t, and o_t are the forget, input, and output gates, respectively. c_t is the cell state at time t. σ_g, σ_c, and σ_h are the sigmoid, hyperbolic tangent, and ReLU activation functions, respectively. W and U are weight matrices, and b is the bias vector.

3. RESULTS AND DISCUSSION

3.1 High-Fidelity CFD Results

A test case is defined by the parameter conditions $T_{N_2}, U_{N_2}, V, D_d, q/m$. T_{N_2}, U_{N_2} and V are the temperature, velocity and voltage of the injected gas that is nitrogen. The last two values are the size of the droplets emitted and the electric charge-to-mass ratio. Although these two can be joined into one, defining the maximum droplet size, the working condition of a specific test case becomes $W_s : \{T_{N_2}, U_{N_2}, V, D_{max}\}$. Reducing the number of parameters that characterize a case helps in the correlations for the machine learning model.

We tested a total of 26 different working conditions. From this dataset, we separated two test cases to use in testing the deep learning model. The two cases for testing the predictions of the model are defined as Test A and Test B, with the conditions in the Table 1. A total number of time steps $N = 120$ was extracted for all simulations. Since the total simulation time is $T = 30$ ms, we extracted snapshots with a time-step of $\delta t = 0.25$ ms.

Figure 4 shows the solution results under different working conditions. Figure 4a and 4b shows the 3D view of the electrospray, showing the temperature and velocity fields on the droplets. Figure 4c shows the droplet's deposition on the target wall, where the droplets are coloured by its diameter.

3.2 Predictions with Deep Learning models

Having the dataset constructed with input X as the temporal 2D images of the side view of the spray and output y as images of the final deposition on the target, we designed different deep learning models, considering the previous considerations.

Consider that the initial goal is to find a suitable model that takes N_s snapshots of the side view of the spray at times $t : \{t_1, t_2, \cdots, t_{N_s}\}$ as input, and produces a prediction of the final spray deposition at time $T = 30$ as an image snapshot of the top view of the plate target. This image shows the density of the deposited droplets.

The models were trained using the mean squared error loss function and the Adam optimizer [23] with a learning rate of 0.001. The model's performance was evaluated on the validation set using the mean squared error and mean absolute error metrics. The Mean Squared Error (MSE) and Mean Absolute Error (MAE) metrics for the loss are defined as follows:

$$L_{MSE} = \frac{1}{n}\sum_{i=1}^{n}(y_i - \widehat{y_i})^2, \tag{7}$$

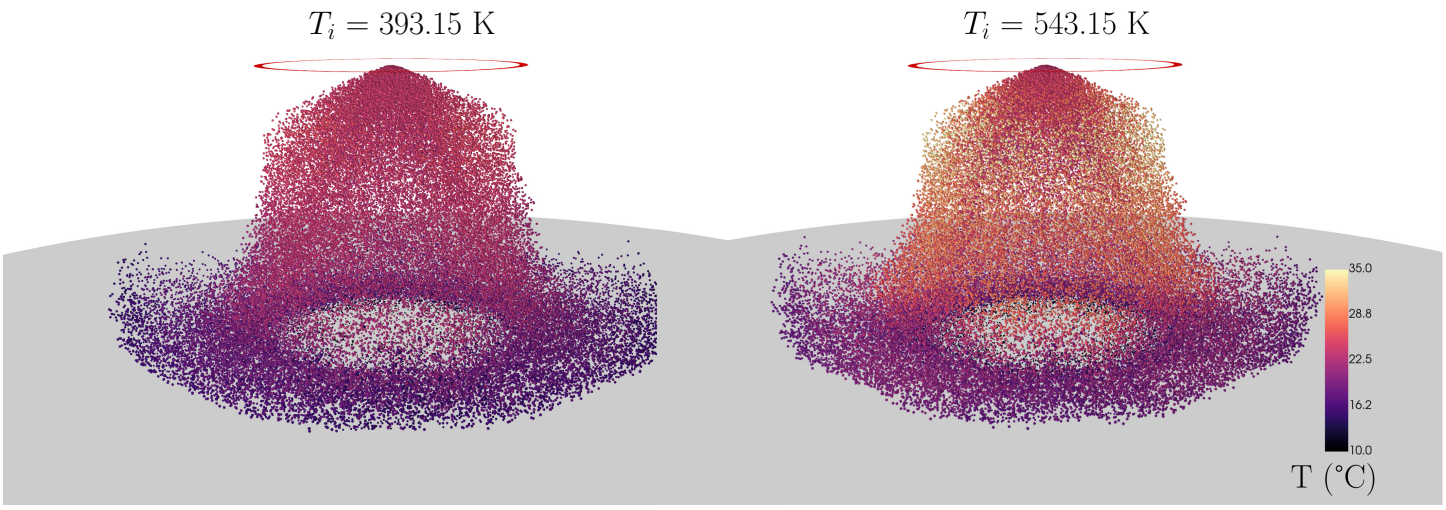

(a)

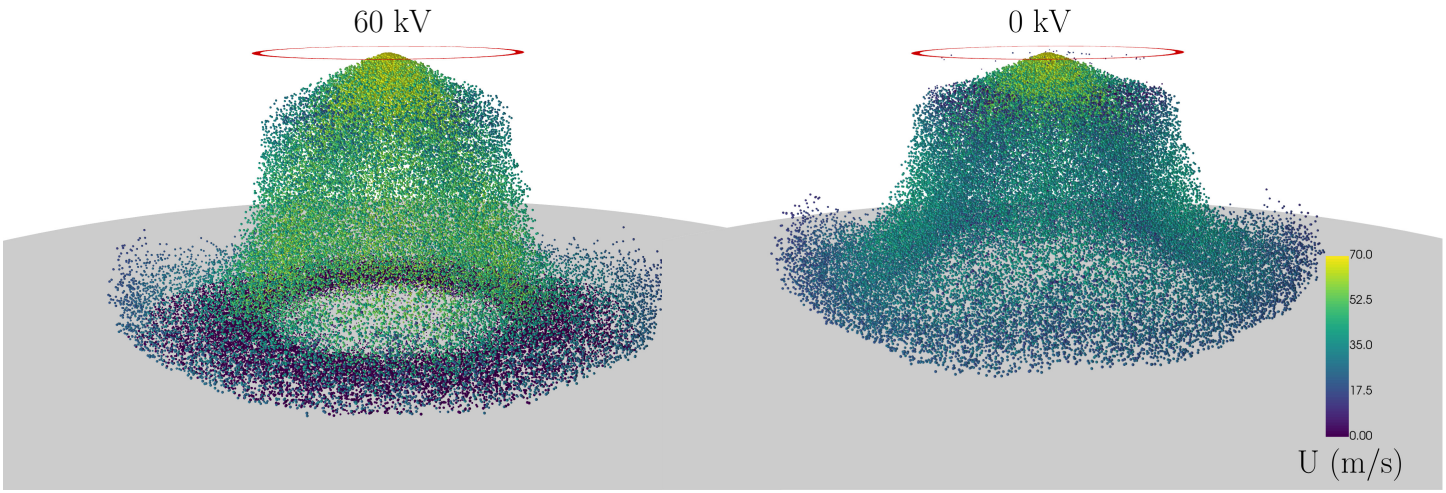

(b)

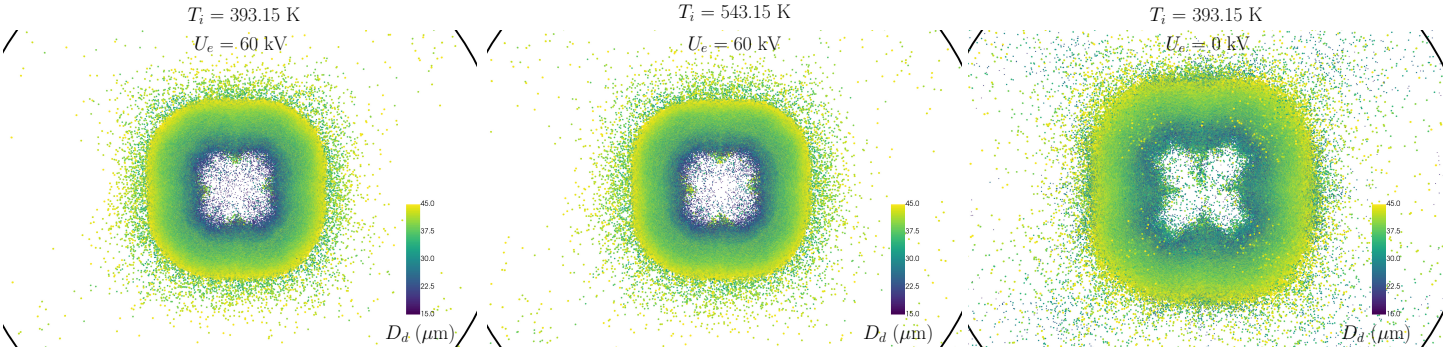

(c)

FIGURE 4: RESULTS FROM 3D EULERIAN-LAGRANGIAN CFD MODEL SHOWING THE (A) INFLUENCE OF THE INLET TEMPERATURE OF THE NITROGEN, COLOURED BY THE TEMPERATURE OF THE DROPLETS (B) INFLUENCE OF THE ELECTRIC POTENTIAL APPLIED, COLOURED BY THE VELOCITY MAGNITUDE OF THE DROPLETS. (C) DROPLET DEPOSITION COLOURED BY THE DROPLET'S DIAMETER.

TABLE 1: WORKING CONDITIONS TESTED FOR DATABASE CONSTRUCTION.

Case no.	T_{N_2} [K]	U_{N_2} [m/s^2]	Φ_e [kV]	$q_{d,max}$ [pC]
Base	393.15	150	60	0.57
Train/Validation	[298.15, 543.15]	[0, 300]	[0, 90]	[0.0,12.30]
Test A	393.15	150	30	0.57
Test B	393.15	150	60	4.58

$$L_{MAE} = \frac{1}{n}\sum_{i=1}^{n} |y_i - \widehat{y_i}|\,, \tag{8}$$

where n is the number of samples, y_i is the true value of the i^{th} sample, and $\widehat{y_i}$ is the predicted value of the i^{th} sample.

The data was divided in $(N_n, N_v, N_t) = (21, 3, 2)$, corresponding to the number of cases for training, validation and testing, respectively. Since our dataset is composed of a small dataset (26 cases), the validation/training was 13%, and the convergence of the models upon the epoch was defined by an early stopping criterion, avoiding overfitting the model's parameters. This criterion stops the training whenever the L_{MSE} error exceeds the minimum reached within 1000 epochs.

An important hyper-parameter of the training is the batch size N_b, which defines the number of samples to be trained from the training set through the network. Since it can affect model convergence, generalization, and computational efficiency, choosing a suitable batch size is crucial in deep learning applications. The choice of batch size is typically influenced by the complexity of the model, the size of the dataset, the hardware's memory capabilities, and the optimization strategy used for training. On the one hand, low values of N_b take a longer time in learning time but with higher accuracy. On the other hand, large values of batch size take a shorter time in learning time but reversely with a lower accuracy [24]. To have the best batch size, we tested the different network architectures for different batch sizes of 1, 2, and 4. Also, we examined for the different models designed and for different sizes of input snapshots. The results are presented in Figure 5a.

Figure 5a shows the loss values for all the different architectures tested. The L_{test} is the MSE error calculated for both test cases (Test A, Test B) and the mean value was obtained. We then observe that a batch size of 1 using LSTM layers leads to a lower range of error. To observe how the batch size affects the training, Figure 5b shows the evolution of the loss on the epochs.

The quantitative comparison between the model architectures, the choice of the number of input snapshots, and the hyperparameters, for the choice of the best ones are done with the MSE and MAE error initially, as we showed. Although since we are dealing with images more than two parameters are used in order to ensure the quality reconstruction of the images. In the field of reconstructing images, there are two parameters that are commonly used. The first is the Structural Similarity Index (SSIM) is a metric used to measure the similarity between two images. It considers the luminance, contrast, and structure of the images. The SSIM is calculated using the following equation,

$$\text{SSIM}\,(x, y) = \frac{\left(2\mu_x\mu_y + c_1\right)\left(2\sigma_{xy} + c_2\right)}{\left(\mu_x^2 + \mu_y^2 + c_1\right)\left(\sigma_x^2 + \sigma_y^2 + c_2\right)} \tag{9}$$

where x and y are the two images being compared, μ_x and μ_y are the mean values, σ_x and σ_y are the standard deviations, σ_{xy} is the covariance, and c_1 and c_2 are constants that are used to stabilize the division. The numerator of the equation measures the similarity in luminance and contrast between the two images, while the denominator measures the similarity in structure. A higher SSIM value indicates a greater similarity between the images.

The other important measurement is the Peak Signal-to-Noise Ratio (PSNR) given by,

$$\text{PSNR} = 10 \cdot \log_{10}\left(\frac{\text{MAX}^2}{\text{MSE}}\right) \tag{10}$$

where, PSNR is the peak signal-to-noise ratio, MAX is the maximum possible pixel value (e.g., 255 for 8-bit images), and MSE is the mean squared error between the original and reconstructed images. The logarithm function is base 10.

To evaluate the performance of our artificial neural network (ANN) and visualize the relationship between these parameters, we generated a heatmap of the pairwise correlation between the different parameters (all of the discussed until this point), see Figure 6.

Pairwise correlation is a statistical method for determining the degree and direction of a linear relationship between two quantitative variables. The correlation coefficient is determined for each pair of variables in a data set in pairwise correlation analysis. The resulting matrix of correlation coefficients demonstrates how each variable in the data set is related to every other variable. The correlation coefficient is a value ranging from -1 to 1, indicating the degree of linear association between two variables. A value of one implies a perfect correlation, in which as one variable grows, the other decreases proportionally. As shown by the resulting map, we see that the error decreases by a rate of 20% with the number of snapshots used, and the batch size has a proportion of 17% on the maximum error of the reconstruction.

With these results, we chose the model that uses LSTM layers, with a number of input snapshots of 12 and a batch size of 2. After training the model, we predicted the droplet deposition for Test A and Test B. For Test A, we obtained the results shown in Figure 7. The figure compares the CFD results with the predictions made by the ML model. Notice that we chose two very different working conditions in order to test the model's

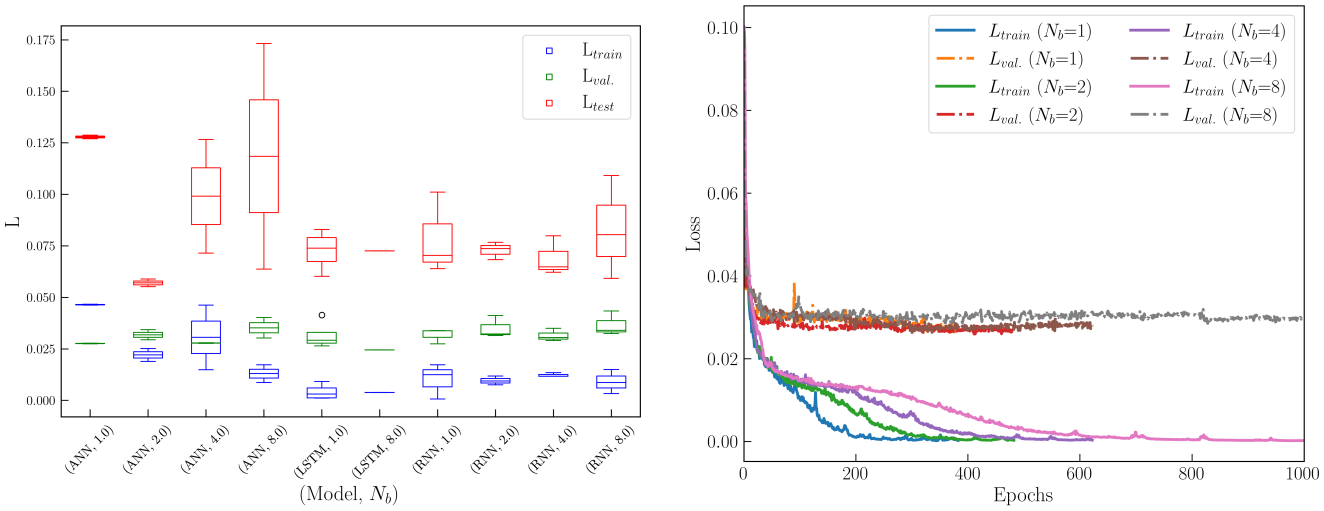

(a) (b)

FIGURE 5: (A) COMPARISON OF THE LOSS ON THE TRAINING, VALIDATION AND TEST SET, FOR ALL THE DEEP LEARNING MODELS TESTED (ANN, RNN, AND LSTM). (B) EVOLUTION OF THE LOSS DURING THE TRAINING FOR THE MODEL OF LSTM.

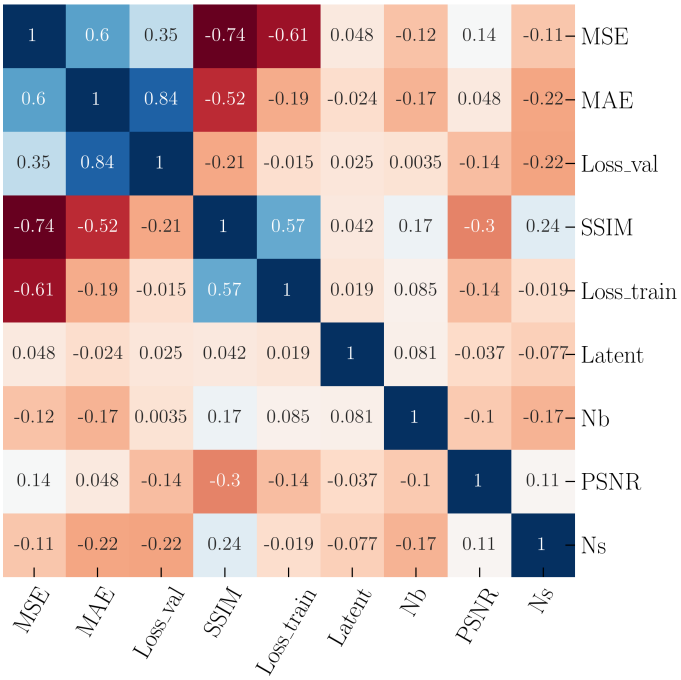

FIGURE 6: HEATMAP OF THE PAIRWISE CORRELATIONS BETWEEN THE DIFFERENT PARAMETERS USED FOR EVALUATION OF THE DEEP MACHINE LEARNING MODEL.

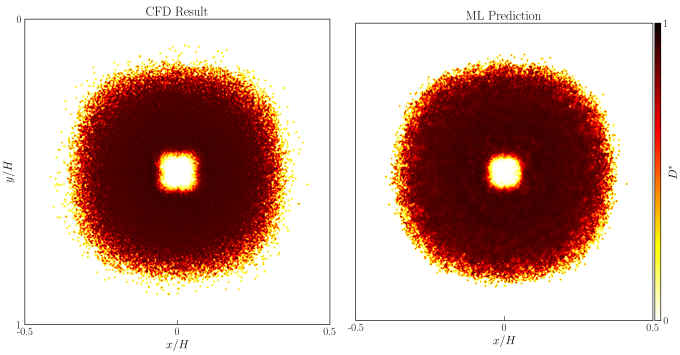

FIGURE 7: PREDICTION OF THE TARGET'S DROPLET'S DEPOSITION FOR THE WORKING CONDITIONS OF THE TEST CASE B.

generalization ability. The results show very good prediction performance, with the core and shape being precisely captured and the error only occurring at the edges. Although there were errors in the droplets scattered by the velocity field, it is important to note that what really matters is capturing the core, which is the region of high density.

Having the prediction of the unseen test cases, we now see where the difference is between the prediction and the real CFD solution in Figure 8. As we can observe, the main core of the target's deposition is accurately predicted. The edges of the droplet's distribution are the region that has more differences, although these are very tiny droplets that are not significant for the overall prediction.

Since the goal is to predict the area of deposited droplets on the target, we calculate the final error of accuracy by the area of droplets of the CFD vs. the ML prediction, as,

$$\epsilon_A = |A_{ML} - A_{CFD}| / A_{CFD} \tag{11}$$

Having a maximum error of 0.877% for the deposited droplets on

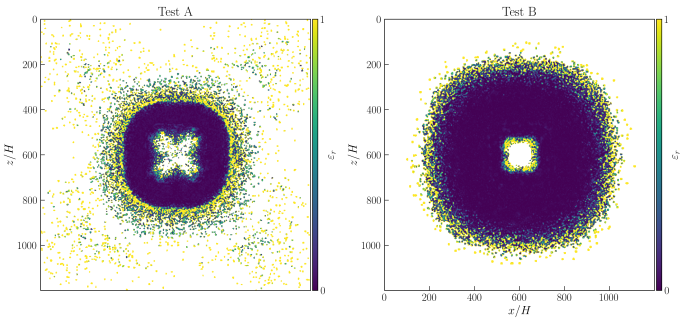

FIGURE 8: ERROR ON THE PREDICTION OF THE TARGET'S DROPLET'S DEPOSITION FOR THE WORKING CONDITIONS OF THE TEST CASE A (LEFT) AND TEST CASE B (RIGHT).

the target for the Test A. This very low error is very promising, for fast simulation of this type of fluid dynamic problems.

4. CONCLUSION

In this paper, we developed a deep-learning model designed to reduce computational time and obtain accurate results for two important aspects of our Eulerian-Lagrangian flow dynamics case. Our machine-learning model analyzes two-dimensional images of snapshots of the spray distributions, from both the side view and top view. We tested different architectures of artificial neural networks and found that when dealing with time-series data, recurrent layers significantly improve the accuracy of the predictions. Our findings show that adding recurrency to the encoding/decoding layers helps with the extraction of features, since we have temporal inputs, where RNN/LSTM cells were implemented. From the results, we observed that the RNN network is more sensitive to the batch size N_b compared to the LSTM network.

In summary, this paper introduces a deep-learning model that demonstrates the ability to make accurate predictions. Our results show that we can reduce the computation time by 90%. By computing the initial evolution of the nitro-thermal spray using CFD (which accounts for only 10% of the full spray evolution), we can predict the final shape of the deposition on the target with an error of approximately 1% for the area of the deposited liquid.

ACKNOWLEDGMENTS

This work was supported by R&D Project "GreenAuto: Green innovation for the Automotive Industry", founded by the incentive system "Agendas Mobilizadoras para a Inovação Empresarial" and Project "MOSIPO", project grant no. POCI-01-0247-FEDER-072621. The research was also partly supported by CMAST Center for Mechanical and Aerospace Science and Technology, research unit No. 151 (Project UID/00151/2020) from Fundacao para a Ciencia e Tecnologia (Portugal). Sílvio Cândido was also supported with national funds by FCT, Foundation for Science and Technology, I.P., through the individual research grant 2020.04517.BD.

REFERENCES

[1] Akafuah, Nelson K., Poozesh, Sadegh, Salaimeh, Ahmad, Patrick, Gabriela, Lawler, Kevin and Saito, Kozo. "Evolution of the automotive body coating process-A review." *Coatings* Vol. 6 (2016). DOI 10.3390/coatings6020024.

[2] Pendar, Mohammad Reza, Rodrigues, Frederico, Páscoa, José Carlos and Lima, Rui. "Review of coating and curing processes: Evaluation in automotive industry." *Physics of Fluids* Vol. 34 (2022). DOI 10.1063/5.0109376.

[3] Spang, Peter. "Applying Paints with Nitrogen." *IST International Surface Technology* Vol. 7 (2014). DOI https://doi.org/10.1365/s35724-014-0220-0.

[4] Bensalah, W., Loukil, N., Wery, M. De Petris and Ayedi, H. F. "Assessment of automotive coatings used on different metallic substrates." *International Journal of Corrosion* Vol. 2014 (2014). DOI 10.1155/2014/838054.

[5] Kochkov, Dmitrii, Smith, Jamie A, Alieva, Ayya, Wang, Qing, Brenner, Michael P, Hoyer, Stephan, Bertozzi, Andrea L, Designed, S H, Performed, S H and Data;, S H Analyzed. "Machine learning-accelerated computational fluid dynamics." (2021)DOI 10.1073/pnas.2101784118/-/DCSupplemental.y.

[6] Yang, Kwang Tzu. "Artificial Neural Networks (ANNs): A new paradigm for thermal science and engineering." *Journal of Heat Transfer* Vol. 130 (2008). DOI 10.1115/1.2944238.

[7] Cândido, Sílvio and Páscoa, José C. "Numerical Analysis of Interfacial Electrohydrodynamic Flow With Modal Decomposition." Vol. Volume 8: Fluids Engineering; Heat Transfer and Thermal Engineering (2022): p. V008T10A004. DOI 10.1115/IMECE2022-95100.

[8] Cortes, Corinna, Vapnik, Vladimir and Saitta, Lorenza. "Support-Vector Networks Editor." *Machine Leaming* Vol. 20 (1995): pp. 273–297.

[9] Hochreiter, Sepp and Schmidhuber, Jürgen. "Long Short-Term Memory." *Neural Computation* Vol. 9 No. 8 (1997): pp. 1735–1780. DOI 10.1162/neco.1997.9.8.1735.

[10] Lecun, Yann, Bengio, Yoshua and Hinton, Geoffrey. "Deep learning." *Nature* Vol. 521 (2015): pp. 436–444. DOI 10.1038/nature14539.

[11] Naphon, P., Wiriyasart, S., Arisariyawong, T. and Nakharintr, L. "ANN, numerical and experimental analysis on the jet impingement nanofluids flow and heat transfer characteristics in the micro-channel heat sink." *International Journal of Heat and Mass Transfer* Vol. 131 (2019): pp. 329–340. DOI 10.1016/j.ijheatmasstransfer.2018.11.073.

[12] Elsayed, Khairy and Lacor, Chris. "Modeling, analysis and optimization of aircyclones using artificial neural network, response surface methodology and CFD simulation approaches." *Powder Technology* Vol. 212 (2011): pp. 115–133. DOI 10.1016/j.powtec.2011.05.002.

[13] Zafar, Afia, Aamir, Muhammad, Nawi, Nazri Mohd, Arshad, Ali, Riaz, Saman, Alruban, Abdulrahman, Dutta, Ashit Kumar and Almotairi, Sultan. "A Comparison of Pooling Methods for Convolutional Neural Networks." *Applied Sciences (Switzerland)* Vol. 12 (2022). DOI 10.3390/app12178643.

[14] Lusch, Bethany, Kutz, J. Nathan and Brunton, Steven L. "Deep learning for universal linear embeddings of nonlinear dynamics." (2017)DOI 10.1038/s41467-018-07210-0.

[15] Brunton, Steven L., Proctor, Joshua L., Kutz, J. Nathan and Bialek, William. "Discovering governing equations from data by sparse identification of nonlinear dynamical systems." *Proceedings of the National Academy of Sciences of the United States of America* Vol. 113 (2016): pp. 3932–3937. DOI 10.1073/pnas.1517384113.

[16] Graves, Alex. "Generating Sequences With Recurrent Neural Networks." (2013).

[17] Yousif, Mustafa Z., Yu, Linqi, Hoyas, Sergio, Vinuesa, Ricardo and Lim, HeeChang. "A deep-learning approach for reconstructing 3D turbulent flows from 2D observation data." (2022)DOI 10.1038/s41598-023-29525-9. URL http://arxiv.org/abs/2208.05754.

[18] Cândido, Sílvio and Páscoa, José C. "Dynamics of three-dimensional electrohydrodynamic instabilities on Taylor cone jets using a numerical approach." *Physics of Fluids* Vol. 35 No. 5 (2023): p. 052110. DOI 10.1063/5.0151109.

[19] Pendar, Mohammad Reza and Páscoa, José Carlos. "Numerical modeling of electrostatic spray painting transfer processes in rotary bell cup for automotive painting." *International Journal of Heat and Fluid Flow* Vol. 80 (2019). DOI 10.1016/j.ijheatfluidflow.2019.108499.

[20] Pendar, Mohammad Reza and Páscoa, José Carlos. "Atomization and spray characteristics around an ERBS using various operational models and conditions: numerical investigation." *International Journal of Heat and Mass Transfer* Vol. 161 (2020). DOI 10.1016/j.ijheatmasstransfer.2020.120243.

[21] Pendar, Mohammad Reza and Páscoa, José Carlos. "Numerical analysis of charged droplets size distribution in the electrostatic coating process: Effect of different operational conditions." *Physics of Fluids* Vol. 33 (2021). DOI 10.1063/5.0041021.

[22] Pendar, Mohammad-Reza, Cândido, Sílvio and Páscoa, José Carlos. "Optimization of painting efficiency applying unique techniques of high-voltage conductors and nitrotherm spray: Developing deep learning models using computational fluid dynamics dataset." *Physics of Fluids* Vol. 35 No. 7 (2023): p. 075119. DOI 10.1063/5.0156571.

[23] Kingma, Diederik P. and Ba, Jimmy. "Adam: A Method for Stochastic Optimization." (2014).

[24] Zhang, Yonggang and Yang, Lining. "A novel dynamic predictive method of water inrush from coal floor based on gated recurrent unit model." *Natural Hazards* Vol. 105 (2021): pp. 2027–2043. DOI 10.1007/s11069-020-04388-9.